HHS Public Access

Author manuscript

Proc SPIE Int Soc Opt Eng. Author manuscript; available in PMC 2015 May 13.

Published in final edited form as:

Proc SPIE Int Soc Opt Eng. 2015 March 9; 9332: 93320R–. doi:10.1117/12.2076300.

Design and validation of a diffuse reflectance and spectroscopic microendoscope with poly(dimethylsioxane)-based phantoms

Gage J. Greening[1], **Amy J. Powless**[1], **Joshua A. Hutcheson**[1], **Sandra P. Prieto**[1], **Aneeka A. Majid**[1], and **Timothy J. Muldoon**[1]

[1]Department of Biomedical Engineering, University of Arkansas, Fayetteville, AR, USA 72701

Abstract

Many cases of epithelial cancer originate in basal layers of tissue and are initially undetected by conventional microendoscopy techniques. We present a bench-top, fiber-bundle microendoscope capable of providing high resolution images of surface cell morphology. Additionally, the microendoscope has the capability to interrogate deeper into material by using diffuse reflectance and broadband diffuse reflectance spectroscopy. The purpose of this multimodal technique was to overcome the limitation of microendoscopy techniques that are limited to only visualizing morphology at the tissue or cellular level. Using a custom fiber optic probe, high resolution surface images were acquired using topical proflavine to fluorescently stain non-keratinized epithelia. A 635 nm laser coupled to a 200 μm multimode fiber delivers light to the sample and the diffuse reflectance signal was captured by a 1 mm image guide fiber. Finally, a tungsten-halogen lamp coupled to a 200 μm multimode fiber delivers broadband light to the sample to acquire spectra at source-detector separations of 374, 729, and 1051 μm. To test the instrumentation, a high resolution proflavine-induced fluorescent image of resected healthy mouse colon was acquired. Additionally, five monolayer poly(dimethylsiloxane)-based optical phantoms with varying absorption and scattering properties were created to acquire diffuse reflectance profiles and broadband spectra.

Keywords

diffuse; reflectance; spectroscopy; microendoscopy; phantoms; fiber; proflavine

1. INTRODUCTION

White light endoscopy is the standard of care for imaging body organs like the oral cavity, esophagus, gastrointestinal tract (colonoscopy), and cervix (colposcopy).[1–3] Recently, high resolution fiber-bundle microendoscopy has shown high sensitivity and specificity in the detection of several types of epithelial cancers, including oral, colorectal, and cervical cancers. Specimens are typically stained with a fluorescent dye like proflavine to provide nuclear-to-cytoplasmic contrast on a micrometer scale.[4–6] Thus, cell surface morphology can be visualized in greater contrast. White light endoscopy still has major clinical advantages like its wide field of view, so the motive of most high resolution

microendoscopy systems is to serve as an intermediate step between standard white light visual inspection and biopsy, so that the clinician can more accurately pinpoint optimal sites for biopsy. This has the potential to reduce the number of unnecessary biopsies.[4–6] However, one of the limitations to high resolution, fluorescent-based microendoscopy techniques is the inability to detect submucosal abnormalities.[5] To overcome this limitation, we have designed a bench-top, fiber-bundle microendoscope with the capability of both visualizing surface morphology and interrogating deeper into tissue to provide depth-sensitive information. Using a custom fiber optic probe consisting of a central image guide fiber and an array of delivery and collection fibers, this microendoscopy technique can acquire data on proflavine-induced fluorescence, diffuse reflectance spectroscopy (DRS), and bulk tissue diffuse reflectance, of which the latter two modalities provide depth-sensitive data.[7–11]

Proflavine-induced fluorescence has been previously described in many microendoscopy applications in the oral cavity, gastrointestinal tract, and cervix.[4–6] Proflavine is a fluorescent acridine-derived dye that preferentially stains cell nuclei and has been safely used in human gastrointestinal fluorescence imaging research for many years.[5] The peak excitation and emission wavelengths for a solution of proflavine in water are around 440 nm and 510 nm, corresponding to a Stokes shift of approximately 70 nm.[12] In this study, resected healthy murine colon tissue was topically stained with proflavine and excitation was provided by delivering light from a blue, 455 nm LED through an image guide fiber. Emitted fluorescent signal, primarily from the cell nuclei, was captured by a charged coupled device and stored for later image analysis. This modality allows for fluorescent-contrast of tissue surface morphology.

Broadband diffuse reflectance spectroscopy (DRS) is a widely used technique that provides spectral data on light that has penetrated tissue and reflected out. DRS is sensitive to changes in tissue optical properties, namely the absorption and scattering coefficients.[7–11] This modality uses increasing source-detector separations (374, 729, and 1051 μm) to provide spectra at increasing depths.

Similar to DRS is the instrumentation's capability of collecting two-dimensional diffuse reflectance profiles by off-axis illumination.[13–15] Instead of analyzing diffuse reflectance using a spectrometer, the image guide used to collect fluorescent signal from proflavine also collects 635 nm light from an off-axis delivery fiber. The image guide of the fiber optic probe thus provides a two-dimensional spatial representation of the diffuse reflectance of the sample.

All modalities (proflavine-induced fluorescence, diffuse reflectance spectroscopy, and bulk tissue diffuse reflectance) were controlled with custom LabVIEW (National Instruments) graphical programing software. Validation experiments using poly(dimethylsiloxane) (PDMS)-based tissue-simulating phantoms and resected healthy murine colon tissue demonstrated the working capability of the DRSME.

2. MATERIALS AND METHODS

2.1 Design of the diffuse reflectance and spectroscopic microendoscope (DRSME)

The light sources of the imaging system include an LED light source (Luxeon) centered at 455 nm (20 nm FWHM), a broadband tungsten-halogen white light source (Ocean Optics), and a 635 nm laser (Thorlabs) which are all delivered to the sample via a custom-designed fiber-optic bundle (Myriad Fiber Imaging).

The custom-designed fiber-optic bundle consists of one central image guide fiber (Fujikura Image Fiber, Myriad Fiber Imaging) that has an image circle of 1,025 ± 80 μm and a cladding diameter of 1,100 ± 80 μm. Surrounding the central image guide fiber are five silica core/cladding multimode fibers (Polymicro Technologies) with a 200 ± 4 μm core diameter and 220 ± 4 μm cladding diameter. All individual fibers were contained within a single probe at the distal end of the fiber bundle. At the proximal end of the fiber bundle, all individual fibers branch into bundles that terminate in an SMA905 connector (Thorlabs) to be connected to the DRSME instrumentation. At the distal probe tip, the center of each 200 μm core multimode fiber is 864 μm from the center of the image guide fiber and are spaced 25° apart. Based on this geometry and using the leftmost 200 μm core multimode fiber as a reference, four source-detector separations (SDS) for broadband DRS measurements are potentially possible (374, 729, 1051, and 1323 μm). Figure 1 shows an overall schematic of the DRSME instrumentation as well as images of the associated fiber-optic bundle. Additionally, Fig. 1 explicitly shows the individual fiber positions at both the proximal and distal ends of the fiber-optic bundle.

To create proflavine fluorescence images, light from the 455 nm LED is coupled through the central image guide fiber to the sample. First, 455 nm LED light passes through a 460 nm short pass excitation filter (Chroma Technology Corp.) and is directed into the back aperture of a 10X/0.30 NA infinity-corrected objective lens (Olympus) using a 475 nm cut-off dichroic mirror (Chroma Technology Corp.). Blue excitation light passes through the 1,025/1,200 μm image guide to the distal end of the probe, illuminating the sample with 1 mW of power. Samples fluorescently stained with proflavine excite and emit light centered at approximately 510 nm which is also collected by the image fiber (epi-illumination). Most of the emitted green light passes through the 475 nm dichroic mirror and is reflected by a second dichroic mirror with a cut-off of 590 nm. Reflected green emission light then passes through a 525/40 nm emission filter (Chroma Technology Corp.), a 50 mm achromatic doublet tube lens (Thorlabs), and into a Flea3 USB3 monochrome CCD (Point Grey).

To obtain broadband diffuse reflectance spectral (DRS) measurements, light from a tungsten-halogen lamp (Ocean Optics) is coupled into one 200/220 μm multimode fibers (the fiber labeled “1” in Fig. 1c) of the fiber-optic probe bundle via a custom-designed motorized optical switch. Within the sample, broadband light undergoes sub-diffuse reflectance events and emitted light is collected by the by the adjacent 200/220 μm multimode fibers (the fibers labeled “2, 3, and 4” in Fig. 1c). The adjacent fibers deliver diffusely reflected broadband light from the three channels of increasing SDS (374, 729, and 1051 μm) to a USB2000+VIS-NIR spectrometer (Ocean Optics).

To collect diffuse reflectance profiles, a 635 nm laser is directly coupled through a 200/220 μm multimode fiber of the custom-designed fiber-optic probe, which delivers the 635 nm light to the sample. Within the sample, this red laser light undergoes sub-diffuse reflectance events and emitted light is collected by the by the 1,025/1,200 μm image guide fiber.[13–15] 635 nm emitted light passes through both the 475 nm and 590 nm cut-off dichroic mirrors, before being reflected by a 1-inch aluminum mirror (Thorlabs). 635 nm light then passes through a 610 nm long pass emission filter (Chroma Technology Corp.), a 50 mm achromatic doublet tube lens (Thorlabs), and into a second Flea3 USB3 monochrome CCD (Point Grey). All modalities are controlled and acquired with a custom LabVIEW user-interface (National Instruments).

2.2 Design of PDMS-based tissue simulating phantoms

Phantoms were constructed with PDMS (Sylgard 184 Silicone Elastomer Kit, Dow Corning, USA) as the substrate material. Absorption properties were controlled by adding distilled alcohol-soluble nigrosin (Sigma-Aldrich, USA, SKU: 211680-25G) to PDMS.[16] Alcohol-soluble nigrosin comes in black powdered form and was distilled with ethanol to create a 1% w/v nigrosin/ethanol solution. Scattering properties were controlled by adding titanium dioxide (Sigma-Aldrich, USA, SKU: 718467-100G) to PDMS.[17] Curing agent was added to the mixture in a 10:1 curing agent:elastomer base ratio as recommended by the manufacturer. All components were mixed in a previously described method.[18] Three 1.5 centimeter thick monolayer phantom layers were constructed with a constant concentration of 1% w/v nigrosin/EtOH (5.0 μL/g PDMS) and a varying concentration of TiO_2 (4.0, 8.0, and 12.0 mg/g PDMS). Two more 1.5 centimeter thick monolayer phantom layers were constructed so that three total phantoms had a constant concentration of TiO_2 (8.0 mg/g PDMS) and a varying concentration of 1% w/v nigrosin/EtOH (2.5, 5.0, and 10.0 μL/g PDMS). Table 1 lists the concentrations of absorbing and scattering agent used for each phantom. Figure 2 shows a picture of each constructed phantom.

2.3 Image acquisition and data analysis protocol

All five phantoms from Table 1 and Figure 2 were placed in direct contact with the fiber-optic probe tip. Proflavine-induced fluorescence imaging was not applicable for phantoms. Instead, 635 nm laser light was delivered the phantom and diffusely reflected light was captured by the CCD camera. Exposure was 100 milliseconds and gain was 15. Incident laser power at the sample was maintained at 0.85 mW. One diffuse reflectance profile from each phantom was used for analysis. Immediately following this, broadband light was delivered to the phantom and diffusely reflected light at three SDS (374, 729, and 1051 μm) was captured by a spectrometer. At each SDS, the integration time of the spectrometer was 2 seconds. Incident lamp power at the sample was maintained at 0.15 mW. 15 spectra from each phantom at each SDS was acquired and averaged. Following this, averaged spectra were calibrated with a spectralon-based diffuse reflectance standard (Ocean Optics) and normalized.

Additionally, proflavine-induced fluorescence images were taken of a resected healthy colon from a mouse. After dissection, a 1 cm^2 sample was cut from the mouse colon and placed in a petri dish. Proflavine (0.01% w/v in saline) was topically applied to the resected tissue and

placed in direct contact with the fiber-optic probe tip. 455 nm LED was coupled to the probe and fluorescent signal was captured by the CCD camera. Exposure was 100 milliseconds and gain was 10. Incident LED power at the sample was maintained at 1 mW. Images of the mouse colon taken in this way were used for qualitative analysis. Figures 3 and 4 demonstrate the capabilities of the DRSME.

3. RESULTS AND DISCUSSION

Figure 3 demonstrates the three modalities of the DRSME, including a proflavine-induced fluorescence image of murine colonic glandular structure and a diffuse reflectance profile and spectrum of Phantom #2 from Table 1. Figure 3(A) is not meant for quantitative analysis or for comparison with the diffuse reflectance data from Fig. 3(B–C). For the diffuse reflectance spectra in Fig. 3(C), normalized and calibrated data from the 374 μm (shallow) channel is provided.

Figure 4 shows the quantification of the diffuse reflectance and DRS modalities of the DRSME instrumentation. Demonstrated in this figure are the raw, color-mapped diffuse reflectance profiles of all five PDMS-based tissue simulating phantoms with associated labels. Phantoms 1–3 were made with an increased amount of scattering agent (TiO_2) and constant absorbing agent. Phantoms 4, 2, and 5 were made with an increased amount of absorbing agent (1% w/v nigrosin/EtOH) and constant scattering agent.

Diffuse reflectance profiles in Fig. 4(A–B) were quantified in Matlab by taking a line plot through the central horizontal axis and then fitting the plot to a 3-degree polynomial. The line plot in Fig. 4(C–D) were taken between 400 and 1300 μm (900 μm width) from the center of the 635 nm laser delivery fiber, effectively cutting off noise around the edge of the diffuse reflectance profile due to artifacts from the cladding of the image guide fiber. This concept can be more clearly visualized in the inset diffuse reflectance profile in Fig. 4(C–D). Finally, the line plots of the diffuse reflectance profiles were normalized with respect to the profile with the most intense reflectance signal.

As seen in Fig. 4(C), increasing the concentration of TiO_2 increased the overall diffuse reflectance signal, and this difference was especially prominent in regions closer to the delivery fiber (near the 400 μm source-detector separation). Alternatively, Fig 4(D) shows that increasing the concentration of 1% w/v nigrosin/EtOH decreased the overall diffuse reflectance signal. The difference between phantoms with different absorber concentrations was not as strikingly prominent in regions closer to the delivery fiber (near the 400 μm source-detector separation) when compared to regions further from the delivery fiber (near the 1300 μm source-detector separation).

Next, diffuse reflectance spectra were compared in Fig. 4(E–F). 15 spectra were taken of each of the five phantoms, averaged, and calibrated with a spectralon-based reflectance standard. The spectra were normalized with respect to the spectra with the most intense signal. Fig. 4(E) shows that increasing the concentration of TiO_2 increased the intensity of the spectra across all wavelengths. Fig. 4(F) shows a similar trend in which increasing the concentration of 1% w/v nigrosin/EtOH decreased the intensity of the spectra across all wavelengths in a similar trend. The spectra showed a peak around the 400 nm region and

then began to decline until beginning to steady between 500 to 900 nm. The intensity of the spectra then began to rise at 900 nm. The higher spectral intensity between the 400 to 500 nm wavelength regions corresponds to the blue-hued phantoms shown in Fig. 2.

4. CONCLUSION

We have presented a multi-modal optical imaging device called a diffuse reflectance and spectroscopic microendoscope (DRSME) capable of successive acquisition of proflavine-induced fluorescence, diffuse reflectance, and diffuse reflectance spectroscopy (DRS) using a simple probe design. The motivation for this instrumentation is to provide data on surface morphology as well as sub-surface tissue properties. To demonstrate the working capability of the DRSME, we imaged the glandular structure of resected murine colon tissue and acquired diffuse reflectance data on five PDMS-based tissue simulating phantoms. Following initial validation, diffuse reflectance profiles will be compared to several Monte Carlo models that simulate diffuse reflectance.[19, 20] Other future steps include *ex vivo* imaging of $Apc^{Min/+}$ mice at progressive stages of cancer development in the gastrointestinal tract using all image modalities. Resected colorectal tissue from $Apc^{Min/+}$ mice will be placed on PDMS-based tissue simulating phantoms with comparable optical properties.[21] For these experiments, the absorption and reduced scattering coefficients of phantoms can be directly quantified using methods such as spatial frequency domain imaging.[18, 22]

References

1. Wang TD, Van Dam J. Optical Biopsy: A New Frontier in Endoscopic Detection and Diagnosis. Clinical Gastroenterology and Hepatology. 2004; 2(9):744–753. [PubMed: 15354274]
2. Subramanian V, Ramappa V, Telakis E, et al. Comparison of high definition with standard white light endoscopy for detection of dysplastic lesions during surveillance colonoscopy in patients with colonic inflammatory bowel disease. Inflammatory Bowel Diseases. 2013; 19(2):350–355. [PubMed: 22552948]
3. Sami SS, Subramanian V, Butt WM, et al. High definition versus standard definition white light endoscopy for detecting dysplasia in patients with Barrett's esophagus. Diseases of the Esophagus. 2014
4. Quinn MK, Bubi TC, Pierce MC, et al. High-Resolution Microendoscopy for the Detection of Cervical Neoplasia in Low-Resource Settings. PLOS One. 2012; 7(9)
5. Muldoon TJ, Roblyer D, Williams MD, et al. Noninvasive imaging of oral neoplasia with a high-resolution fiber-optic microendoscope. Head & Neck. 2012; 34(3):305–312. [PubMed: 21413101]
6. Parikh N, Perl D, Lee MH, et al. In vivo diagnostic accuracy of high resolution microendoscopy in differentiating neoplastic from non-neoplastic colorectal polyps: a prospective study. The American Journal of Gastroenterology. 2014; 109(1):65–75.
7. Yu B, Fu HL, Ramanujam N, et al. Instrument independent diffuse reflectance spectroscopy. Journal of Biomedical Optics. 2010; 16(1)
8. Schwarz RA, Gao W, Daye D, et al. Autofluorescence and diffuse reflectance spectroscopy of oral epithelial tissue using a depth-sensitive fiber-optic probe. Applied Optics. 2008; 47(6):825–834. [PubMed: 18288232]
9. Wang HW, Jiang JK, Lin CH, et al. Diffuse reflectance spectroscopy detects increased hemoglobin concentration and decreased oxygenation during colon carcinogenesis from normal to malignant tumors. Optics Express. 2009; 17(4):825–834.
10. Yu B, Shah A, Nagarajan VK, et al. Diffuse reflectance spectroscopy of epithelial tissue with a smart fiber-optic probe. Biomedical Optics Express. 2014; 5(3):675–689. [PubMed: 24688805]

11. Lim L, Nichols B, Rajaram N, et al. Probe pressure effects on human skin diffuse reflectance and fluorescence spectroscopy measurements. Journal of Biomedical Optics. 2011; 16(1)
12. Prahl, S. Proflavine. Oregon Medical Laser Center, December 15, 2014. 2012. http://omlc.org/spectra/PhotochemCAD/html/078.html
13. Kokhanovsky AA. Reflection of light from semi-infinite turbid media. Journal of the Optical Society of America. 1998; 15(11)
14. Graaff R, Aarnoudse JG, Zijp JR, et al. Reduced light-scattering properties for mixtures of spherical particles: a simple approximation derived from Mie calculation. Applied Optics. 1992; 31(10):1370–1376. [PubMed: 20720767]
15. Jacques SL. Optical properties of biological tissues: a review. Physics in Medicine and Biology. 2013; 58(11)
16. Saager RB, Kondru C, Au K, et al. Multi-layer silicone phantoms for the evaluation of quantitative optical techniques in skin imaging. Proceedings of SPIE. 2010; 7567
17. de Bruin DM, Bremmer RH, Kodach VM, et al. Optical phantoms of varying geometry based on thin building blocks with controlled optical properties. Journal of Biomedical Optics. 2010; 15(2)
18. Greening GJ, Istfan R, Higgins LM, et al. Characterization of thin poly (dimethylsiloxane)-based tissue simulating phantoms with tunable reduced scattering and absorption coefficients at visible and nearinfrared wavelength. Journal of Biomedical Optics. 2014; 19(11)
19. Martinelli M, Gardner A, Cuccia D, et al. Analysis of single Monte Carlo methods for prediction of reflectance from turbid media. Optics Express. 2011; 19(20)
20. Hayakawa CK, Spanier J, Venugopalan V. Comparative analysis of discrete and continuous absorption weighting estimators used in Monte Carlo simulations of radiative transport in turbid medi. Journal of the Optical Society of America. 2014; 31(2)
21. McNally JB, Kirkpatrick ND, Hariri LP, et al. Task-based imaging of colon cancer in the ApcMin mouse model. Applied Optics. 2006; 45(13)
22. Cuccia DJ, Bevilacqua F, Durkin AJ, et al. Quantitation and mapping of tissue optical properties using modulated imaging. Journal of Biomedical Optics. 2009; 14(2)

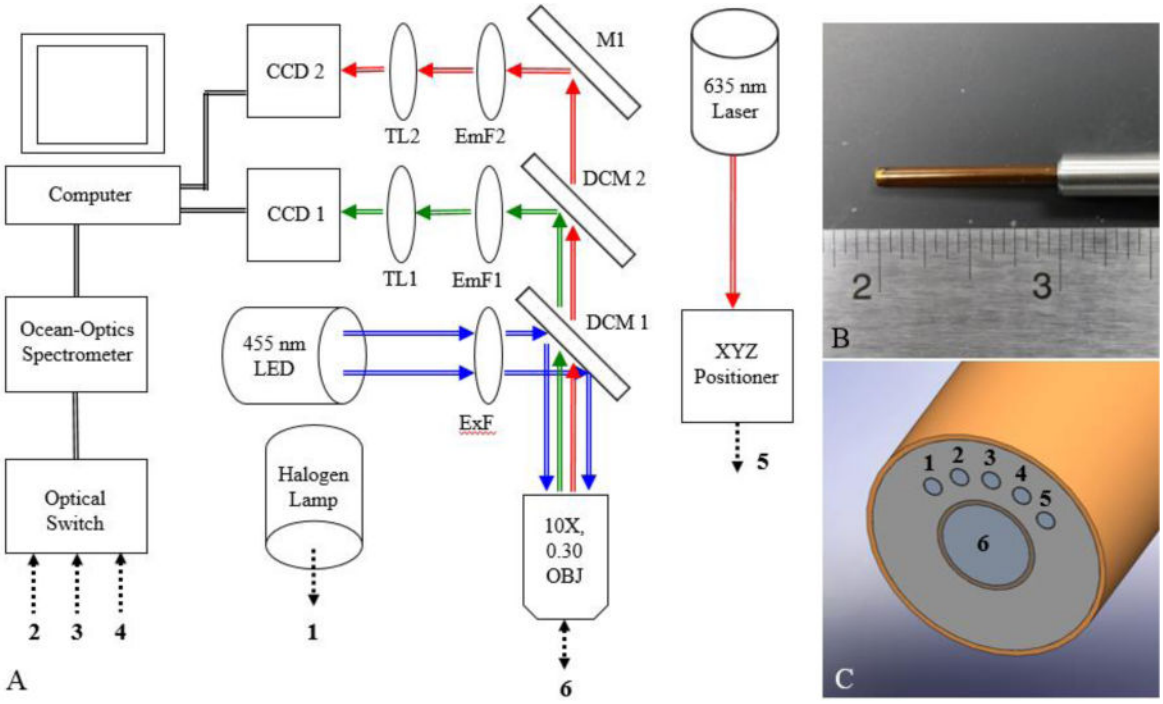

Figure 1.

A representation of the diffuse reflectance and spectroscopic microendoscope (DRSME) showing (A) an instrumentation schematic listing all major components, including numbers (1–6) that indicate the specific fiber number at the proximal end of the fiber-optic probe, (B) an image of the custom-designed fiber-optic probe with a ruler for scale, and (C) a close-up SolidWorks representation of the probe tip with numbers (1–6) that indicate the specific fiber number at the distal end of the fiber-optic probe.

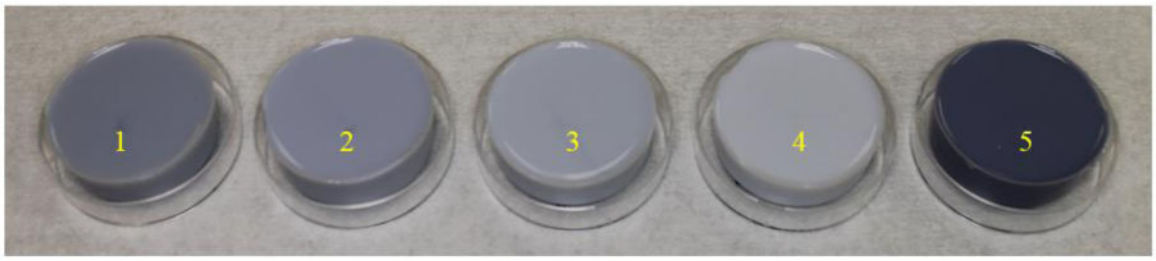

Figure 2.

Image of the PDMS-based tissue-simulating phantoms used in this study. Absorbing agent concentrations (1% w/v nigrosin/EtOH [μL/g]) and scattering agent concentrations (TiO2 [mg/g]) were (1) 5.0 and 4.0, (2) 5.0 and 8.0, (3) 5.0 and 12.0, (4) 2.5 and 8.0, (5) 10.0 and 8.0, respectively.

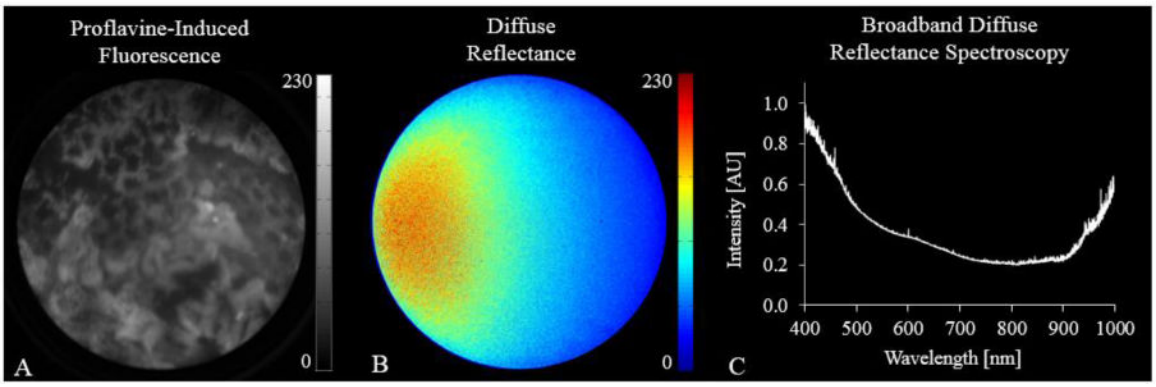

Figure 3.

Representation of the three modalities provided by the diffuse reflectance and spectroscopic microendoscope (DRSME) including (A) a proflavine-induced fluorescence image of healthy, murine colonic epithelium, (B) a diffuse reflectance profile of Phantom 2 (5.0 μL of 1% w/v nigrosin/EtOH per gram PDMS and 8.0 mg TiO_2 per gram PDMS) that was color-mapped using Matlab, and (C) a diffuse reflectance spectrum of the Phantom 2 taken at the same image point with a source-detector separation of 374 μm. The spectrum here was normalized and calibrated with a spectralon-based diffuse reflectance standard from Ocean Optics.

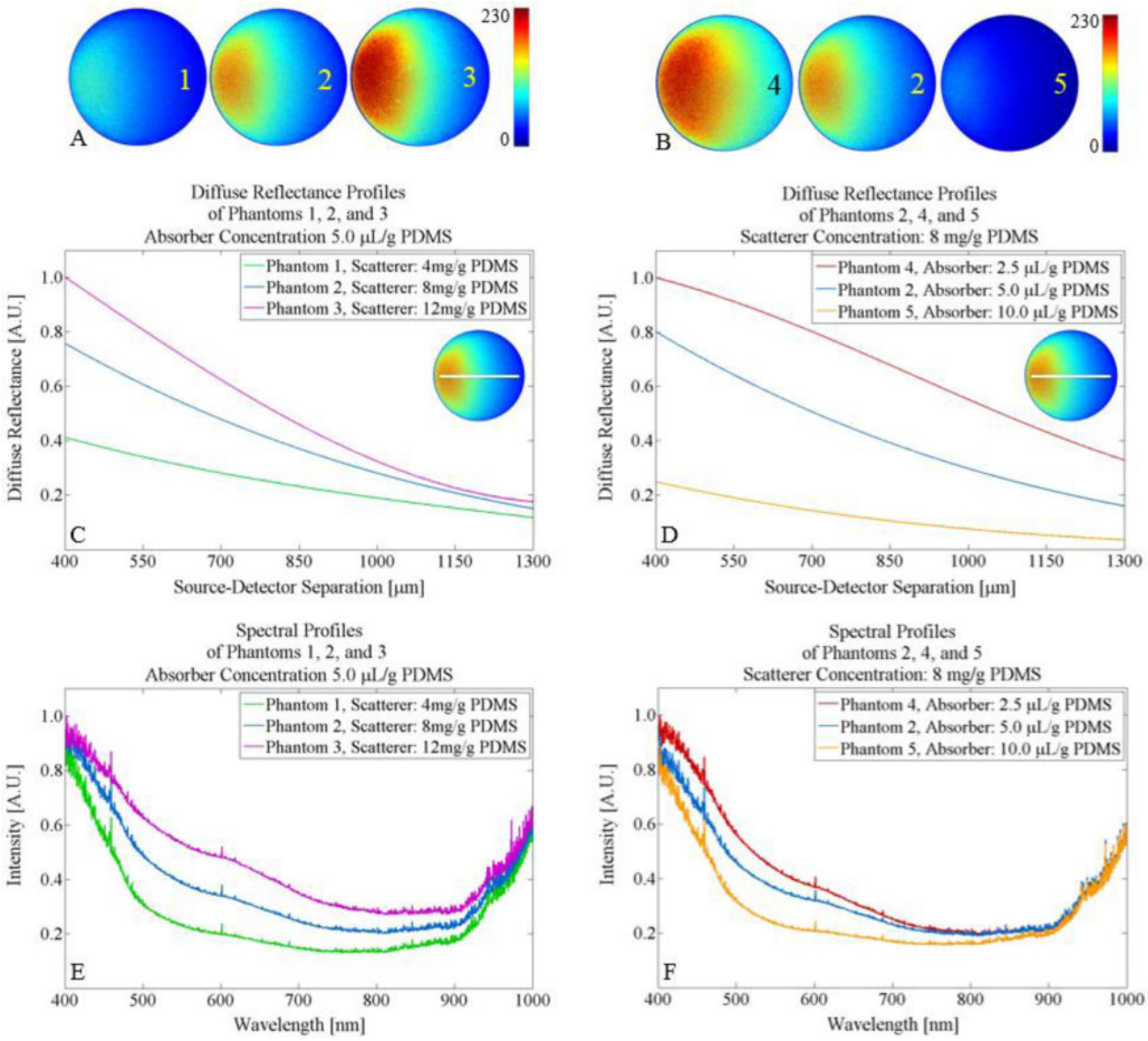

Figure 4.

Quantification of the diffuse reflectance profiles and diffuse reflectance spectra acquired by the DRSME showing (A) diffuse reflectance profiles of Phantoms 1–3 with increased concentration of TiO2, (B) diffuse reflectance profiles of Phantoms 4, 2, and 5 with increased concentration of 1% w/v nigrosin/EtOH, (C) comparison of the diffuse reflectance of Phantoms 1–3 between 400 and 1300 µm from the center of the 635 nm delivery fiber with an inset of line plot through the image guide, (D) comparison of the diffuse reflectance of Phantoms 4, 2, and 5 between 400 and 1300 µm from the center of the 635 nm delivery fiber with an inset of line plot through the image guide, (E) DRS comparison of Phantoms 1–3 between 350–1000 nm, and (F) DRS comparison of Phantoms 4, 2, and 5 between 350–1000 nm.

Table 1

Concentrations of absorbing agent (1% w/v nigrosin/EtOH) and scattering agent (TiO2) used for each layer of the poly(dimethylsiloxane)-based phantoms. Concentrations are in amount of optical agent per weight PDMS.

Phantom Number	Concentration of Absorbing Agent 1% w/v nigrosin/EtOH [μL/g PDMS]	Concentration of Scattering Agent TiO2 [mg/g PDMS]
Phantom 1	5.0	4.0
Phantom 2	5.0	8.0
Phantom 3	5.0	12.0
Phantom 4	2.5	8.0
Phantom 5	10.0	8.0